Exploring extreme rainfall impacts on flow and turbidity dynamics in a steep, pristine and tropical volcanic catchment

Vanessa Solano-Rivera[1], Josie Geris[2], Sebastián Granados-Bolaños[1], Liz Brenes-Cambronero[3], Guillermo Artavia-Rodríguez[1], Ricardo Sánchez-Murillo[4], *Christian Birkel[1,2]

[1]Department of Geography and Water and Global Change Observatory, University of Costa Rica, 2060 San José, Costa Rica.

[2]Northern Rivers Institute, University of Aberdeen, AB24 3UF, Aberdeen, Scotland.

[3]ReBAMB, Sede de Occidente, University of Costa Rica, 2060 San José, Costa Rica.

[4]Stable Isotope Research Group, National University of Costa Rica, Heredia, Costa Rica.

*Corresponding author: christian.birkel@ucr.ac.cr

Manuscript

Abstract: 277 words

Word count: 7164 (without abstract, figure and table captions and reference list)

Number of figures: 9 (colour)

Number of tables: 3

Supplementary material: Figure S1

Abstract

Tropical volcanic landscapes are important because of the short timescales (< years) over which they transform. Sediment sources, availability and transport can be highly dynamic, but our understanding of these is limited by a lack of data in these complex environments, especially with regards to extreme events. To investigate the responses to extreme rainfall events in particular, we conducted extensive monitoring in a pristine tropical rainforest catchment (3.2 km^2), located in the Volcanic Cordillera of Tilarán, Costa Rica. We established high temporal resolution hydro-

meteorological and turbidity monitoring from June 2015 to July 2016. This included a record convective rainfall event in August 2015 which resulted in an estimated > 50 yr return period flood event. We also surveyed hillslope soils, landslides, and sediments of the river network, to characterize sediments before and after the extreme event. Our results suggested that rainfall events activated surface flow pathways with associated mobilization of material. However, erosion processes were mostly linked to finer material (sand, silt) properties of the soils that developed on more highly weathered bedrock. The single extreme event (return period > 50 years) had an overriding impact on the general sediment dynamics. Recovery in the form of fine material transport and associated hysteresis took only about three months. We conclude that the combined use of high-temporal resolution monitoring with spatially distributed surveys provided new insights for the initial assessment into the fluvial geomorphology and transport dynamics of steep, volcanic headwater catchments in the humid tropics with potential to establish more complete time scales of land-forming processes. This work can build the foundation for more complete monitoring using radioisotopes as a tool to fingerprint the sediment origin and composition.

Keywords: Tropics; Costa Rica; turbidity; erosion; Volcanic and fluvial geomorphology; Extreme rainfall events, ReBAMB.

Abbreviations:

AWI7d-	Antecedent wetness 7 days (mm)
M-	Precipitation magnitude (mm)
Imax-	Maximum intensity (mm/h)
P_Qlag-	Lag between the peaks of precipitation and discharge (h)
Range-	Turbidity range from beginning to the event peak (NTU)
P_NTUlag-	Lag between the peaks of precipitation and turbidity (h)
NTU_Qlag-	Lag between the peaks of discharge and turbidity (h)

Qrange Discharge range from beginning to the event peak (m^3/s)

1. Introduction

Tropical ecosystems experience an accelerated land use change (Foley et al., 2005) and are climate change hot spots, particularly in Central America (Giorgi, 2006; González et al., 2017). Despite the deforestation ban in Costa Rica which increased the national forest cover over the last 30 years (Fagan et al., 2013), there is a prevalent trend towards deforestation in the wider region. The associated impacts of these changes on hydrological processes and sediment dynamics in the tropics has received much interest (Chappell et al., 2004; Bonell and Bruijnzeel, 2005). An increasing number of studies have examined sediment dynamics across a wide range of catchments (Fryers, 2013; Buendia et al., 2015). However, these studies have focussed mostly on anthropogenically-impacted catchments (e.g. agriculture), where human disturbance accelerates the natural process of erosion-transport-deposition (Walsh et al., 2011). Research conducted in undisturbed forested areas is limited (see Zhang et al., 2010 as an exception and a global review by Zimmermann et al., 2012), particularly in tropical forests with a geomorphology of volcanic origin (see Muñoz-Villers and McDonnell, 2012, for an example with emphasis on rainfall-runoff dynamics) where the natural dynamics of erosion and deposition processes are mostly unknown.

Furthermore, the tropics are generally characterized by high rainfall rates (Chang and Lau, 1983), which - even under undisturbed vegetation cover - can result in surface flow, erosion and subsequently naturally high sediment loads (Thomas, 1994). In such catchments, the erosion-transport-deposition dynamics tend to be flashy and variable due to the heterogeneity of the climate and the material properties of the soils and bedrock. The soil characteristics with e.g. low hydraulic conductivity, as observed in a lowland rainforest catchment in Panamá, importantly influence the

runoff generation processes with surface flow as the most prominent erosion mechanism (Zimmermann et al., 2012).

Headwater systems globally amount to almost 80% of delivered water and transported substances to rivers (Downing et al., 2012), but remain largely unmonitored. Within the tropics, volcanic landscapes are of specific interest because of the short timescales (< years) over which they transform (Wohl et al., 2012). This may cause severe consequences for downstream water users (e.g. hydropower, drinking water, irrigation, and other ecosystem services). Understanding the formation and evolution of volcanic landscapes in the tropics therefore involves an analysis of the effects of intense and prolonged rainfall events on sediment dynamics and hydrological processes at the event scale. Sediment mobilization can be (initiated) via:

a) shallow landslides and debris flows due to the saturation of the soils contributing material to the streams,

b) laminar erosion on the hillslopes connected to the stream due to surface runoff even under pristine forest cover and

c) the transport dynamics and erosion of the stream, banks and streambed itself.

However, a major challenge in both geomorphology and hydrology is reconciling the disparity between small scale measurements with larger spatial and temporal scale processes (Bracken et al., 2015). One way to assess the integrated response of the system at catchment scales is by linking spatially distributed point scale measurements to high temporal resolution measurements in the stream (Hancock and Lowry, 2015). Alternative approaches include measurements in nested catchments such as by López-Tarazón and Estrany (2016) in the Mediterranean untangling the drivers of sediment transport and their temporal characteristics. Similarly, Mills and Bathurst

(2015) successfully developed a predictive suspended sediment load relationship with spatially distributed catchment characteristics and sediment sources in the UK. However, long-term catchment studies in the tropics are rare (see exceptions from Puerto Rico reported by Shanley et al., 2011 and Thailand by Ziegler et al., 2014), despite that small-scale and detailed measurements may lead to insights into the longer-term landscape forming processes of steep, tropical volcanic catchments and the role extreme events might play.

In Costa Rica, Krishnaswamy et al. (2001a) found that suspended sediment transport was linked to climate dynamics and land use disturbances in a large (~5000 km^2) heterogeneous catchment. In addition, Calvo (1998) attempted to model suspended sediment yields for various larger catchments and found that rainfall erosivity and land use were important drivers of sediment transport. Jansson (2002) explored sediment origin using hysteresis analysis in a meso-scale catchment draining the Caribbean in central Costa Rica. However, these studies followed a relatively coarse temporal resolution (roughly monthly and few events in the case of Jansson, 2002) sampling of suspended sediments, so that the highly dynamic nature of processes during events could not be captured. Following previous larger-scale efforts (e.g. Krishnaswamy et al., 2001b), here, via intense monitoring, we aimed to gain more insights into the sediment transport dynamics in humid tropical volcanic landscapes, with a specific focus on exploring responses to extreme rainfall events. The monitoring included high temporal resolution turbidity, hillslope soil erosion, material properties of soil and sediments, and hydrometric data collected over one hydrological year in the San Lorencito catchment (a 3.2 km^2 tropical pristine headwater catchment) in the Volcanic Cordillera of Tilarán, Costa Rica. Using field and laboratory data and statistical analyses, this study is one of the first in humid tropical volcanic environments that explores when, how and where sediment transport is generated associated with hydrological processes and

catchment responses to intense rainfall events, within the possibilities of a complex and logistically challenging field site. We also tested the utility of turbidity as an indicator of suspended sediment loads in a highly dynamic, volcanic catchment for a relatively short measurement period. The specific objectives were to:

(i) monitor and analyse the stream response and subsequent turbidity dynamics to rainfall inputs at high temporal resolution,

(ii) characterise the impact of an extreme event on the rainfall-runoff-turbidity and sediment relationship, fluvial geomorphology, and the subsequent recovery of the system,

(iii) explore how in-stream dynamics are linked to hillslope sediment sources, their connectivity to the stream, and potential changes to sediment sources induced by extreme events.

2. Study area and methods

2.1. Catchment characteristics

The humid tropical San Lorencito headwater catchment drains an area of 3.2 km^2 towards the Caribbean Sea in the northern mountainous area of Costa Rica known as Cordillera de Tilarán (Figure 1). The catchment is located in the Biological Reserve Alberto Manuel Brenes (ReBAMB), a protected area with restricted access only for research. Land cover involves a typical primary montane rainforest with negligible human intervention (Figure 1e). The most prominent tree species are *Elaegiaux panamensis* and *Ocotea morae*, palmito (*Iriartea deltoidea)* and various types of higuerones (*Ficus spp*.) (Salazar-Rodriguez, 2003).

140 The geology is composed of tertiary volcanic rocks (5-9 million years), mainly from extrusive
141 materials such as basalts, andesites, and pyroclastic flow deposits typical of violent volcanic
142 activity during the younger Miocene Epoch (Bergoeing, 2007) from a nearby emission source in
143 the upper extreme of the catchment (Figure 1b). The morphology of the catchment is characterized
144 by steep slopes (> 30 %). The high annual rainfall is around 3 m/yr with around 2 m/yr of discharge
145 (Table 1). The main stream follows a normal fault line (Figure 1b) resulting in two slightly
146 different main hillslopes. The northern or left hillslope (B, upstream view) shows on average more
147 basalt and more andesitic mineralogy than on the southern or right hillslope (A, Figure 2). Hillslope
148 A is also on average less steep and deeper soils developed compared to those on hillslope B. The
149 soils originating from hillslope A were characterized by loamy and sandy loam particle size, while
150 the soils from hillslope B had less sandy particles and showed some presence of clay (< 30 %).
151 Soil characteristics are related to the volcanic geomorphology of the catchment with less
152 developed, coarse textured Entisols or alluvial soil profiles near the stream. Closer to the hilltops
153 deeper Andisols (> 1 m) with higher organic matter content (> 20 %) and almost permanent
154 saturation can be found. Remnants of volcanic ash in the upper profiles are common (0 – 0.5 m).
155 More information on catchment characteristics and the hydrology of the study site can be found in
156 Dehaspe et al. (2018).

157 The climate is characterized by a constantly high humidity close to 100 % throughout the year
158 with a prolonged rainy season during the months from May to December and a short dry season
159 from January to April. Nevertheless, rain events are common throughout the year (Figure 1d). The
160 study area is situated at the continental divide and is predominantly under the influence of north-
161 eastern trade winds that are responsible for the influx of humidity. The latter in combination with
162 local, intense convective rainstorms generate very high rainfall rates well exceeding 40 mm/h

leading to a rapid stream response. Deviations from normal weather patterns are introduced by frontal systems from the northern hemisphere winter, indirect effects of hurricanes and the El Niño Southern Oscillation (ENSO) resulting in either increased or less rainfall (Birkel et al., 2016).

The San Lorencito stream is highly dynamic and bed materials are generally composed of volcanic angular and sub-angular boulders disposed in large banks along the riverbed. The fluvial geomorphology is dominated by step-pool features with some cascades (Figure 2A and C) and characterized by the occurrence of frequent landslides (Figure 2G) that deposit materials along fluvial terraces (Figure 2F). Stream morphology is also affected by erosion that removes material from the banks and riverbed. Minor alluvial fans can be found along the stream tributaries with available large boulders and sediments to be transported in extreme conditions (Figure 2E).

2.2. Field Measurements and Laboratory Analysis

In-situ sensors measured turbidity (Global Water WQ730, NTU) and water level (Global Water WL400-015-025) in an accessible and relatively protected section at the outlet of the San Lorencito catchment over one year from June 2015 to July 2016. Sensors were placed within a 30kg steel cage and PVC tubes for protection and routinely cleaned and calibrated. Data were stored every 5 minutes using a Global Water GL-500 logger. Meteorological data (rainfall, temperature, humidity, radiation, pressure, wind direction and speed) were measured using a Davis Vantage Pro Plus 2 station (MS1) programmed to 30-min time steps in a cleared spot located 1 km NE outside the study catchment (Figure 3). It is well known that both sloping ground (e.g. Sharon, 1980) and canopy interception (e.g. Loescher et al., 2002) can introduce complexity and variability in the observations of rainfall. To assess the extent to which the complete but single rainfall records of

185 the meteorological station could be used for this study, we therefore initially explored the effects
186 of spatial variability and altitudinal gradients (total elevation gradient is 460m). For this,
187 throughfall measurements (HOBO rain gauges) were taken at different times during the rainy
188 season from June to December 2015 at two locations: one close to the stream (at 890 m a.s.l) and
189 on the left hilltop at 1232 m a.s.l (Figure 2 – MS2 and MS3, respectively). We found that
190 throughfall at MS2 and MS3 and gross precipitation measured at the meteorological station
191 followed identical event timings in terms of peak rainfall with slight differences in measured
192 volumes (< 10 %) due to the intercepting vegetation. No significant precipitation elevation gradient
193 was detected over the relatively short distance that concerns the study site and we do not show this
194 preliminary analysis here. Therefore, we used the continuous measurements of gross rainfall at the
195 meteorological station for further event analysis.

196 Throughout the entire monitoring period, manual discharge gaugings (salt dilution and current
197 meter) were done approximately every 3 weeks and on an occasional event-basis. The difference
198 between both measurement techniques was below 10 % of absolute gauged streamflows. These
199 gaugings were used in the construction of a rating curve that converts measured water level into
200 discharge (m^3/s) (Figure 4). During very high flows (at levels > 0.8 m), overbank flow occurred.
201 We therefore applied a separate rating curve for these higher levels by applying Manning's
202 equation to events with recorded flood marks (four in total). We tested the sensitivity of the
203 resulting discharge estimate by varying the Manning coefficient n for mountain streams with
204 cobbles and large boulders in between a range of 0.04 to 0.07 (Chow, 1959) reported as uncertainty
205 bounds. The maximum discharge was reconstructed for the four largest events and the highest
206 event of the monitoring period, at 10-12 August 2015, with an estimated 50 yr return period. The
207 latter return period is a rough estimate to provide some longer-term context based on the highest

208 recorded rainfall amount and intensity since on-site meteorological measurements began in 2008.
209 Further, the changes to the stream channel were not observed by long-term staff members since
210 the establishment of the research station in 1976. Most importantly, riparian trees (higuerones,
211 *Ficus spp*.) of 30 m height estimated by plant physiologists to exceed 100 years of age were
212 removed by the extreme event. As evidenced by the consistency in gaugings in Figure 4, the
213 channel geometry itself did not change after this large event, so that the same rating curve is applied
214 consistently in time. Uncertainty in the rating curve is highest for the high discharges due to a
215 strong non-linearity induced by the extreme event that exceeds 100-fold the second largest event
216 (Figure 4 inlet). All data were directly used for analysis without gap filling in case of sensor failure.

217 Turbidity measurements were recorded in Nephlometric Turbidity Units (NTU). Continuous, at
218 least monthly, maintenance and cleaning prevented sensor failure. In addition, there was little
219 possibility for debris build-up around the optical sensor due to the high flow velocities (> 2m/s)
220 during events. Stream water samples (n = 23) were manually taken using a standard DH-48
221 sediment sampler across a range of level and turbidity conditions in an attempt to relate the mass
222 of sediments to the NTU data. These stream water samples were processed to obtain the total of
223 suspended and dissolved sediments (American Public Health Association, 1999). The spatial
224 variability in sediments was assessed by collecting manual sediment samples in seven different
225 tributaries on both hillslopes (A, B) and in the main stream (Figure 3). To further determine the
226 impact of main rainfall events, this was done before and after the 50 yr return period flood event.
227 All samples were completely dried for 3 hours at 105 °C, treated with H_2O_2 to remove organic
228 material and then washed and dried again. The sediments were processed to obtain the particle size
229 distribution curve using a set of 19 (Fisher Scientific) sieves varying from 8 to 0.05 mm and the
230 Retsch As200 sieve shaker. The material remaining in each sieve was weighed and visualized as

231 cumulative percentages. The 0.25 mm quartz diameter was selected for a morphoscopic analysis
232 conducted using a Meiji PBH Stand stereoscope (Tricart, 1965). Landslides were mapped after the
233 extreme event and the dimension documented with digital imagery. The landslide volumes were
234 derived from a post-event interpretation of georeferenced photographs converted into 3D imagery
235 using the *Agisoft Photoscan* software.

236 To assess stream sediment in the context of potential source areas, 26 soil samples (0 to 30 cm
237 depth) were taken at accessible sites across the catchment (Figure 3) and analysed for soil texture.
238 Eighteen samples were processed using the pipette method (Veas, 2009) at an earlier time and
239 eight samples using Bouyoucos method over the study period. Despite slight differences in the
240 analytical protocol, both methods provided comparable results using duplicate measurements for
241 comparison (Norambuena et al., 2002). The texture of the soils was determined using the USDA
242 textural triangle (Henríquez & Cabalceta, 2012).

243 To monitor erosion and/or deposition of material on both hillslopes, at different altitudes and
244 slopes, soil movement was assessed using a total of 10 erosion pins following Hancock & Lowry
245 (2015). The pins consisted of 60 cm length steel rods with a > 0.6 cm diameter and were painted
246 with anticorrosive yellow. They were inserted manually (site conditions allowing) without a
247 hammer (Hancock & Lowry, 2015) as depth markers. Readings with an approximate error of 0.2
248 cm were done monthly by the same person during the rainy season and during the dry season the
249 data were collected twice in January and once at the end of May after the rainy season 2016 started.

250

251 **2.3 Statistical Analysis**

We analysed the rainfall-runoff-turbidity dynamics of the study site for a range of different events, which also included a major flood event during August 2015. The identification and definition of an event considered in this study was done systematically and based on both precipitation and discharge data. The start of precipitation indicates the beginning of an event, while the end of the discharge recession curve defined the end of the event. To be able to clearly identify event characteristics, we also imposed a threshold of a minimum water level change of 0.1 m. Double-peak runoff events were not detected.

Descriptive event statistics were used to explore 26 hydro-meteorological variables that characterize the size, range, minimum, maximum, mean, magnitude, intensity, duration of rise and recession and time lag of the precipitation-discharge-turbidity relationship of each selected event, as well as the antecedent wetness conditions for 3, 7 and 30 days plus the time (hours) without rainfall prior to an event. The hysteresis index of Zuecco et al. (2016) was applied using discharge as the independent variable and turbidity as the dependent variable. Among many other hysteresis indices available, the index by Zuecco, et al. (2016) is a dimensionless number allowing for automatic and objective calculation of all the forms of possible hysteresis loops, sizes and directions found here. The selected events were further separated into dry (January to April) and wet (May to December) season and before and after the major event in August 2015 mainly due to the climatic seasonality of the study site and the impact caused by the event.

Spearman rank correlation (r) and Principal Components Analysis (PCA) were applied to reduce the number of environmental variables avoiding co-linearity as indicated by an $r > 0.7$ and to search for relationships that could potentially explain the rainfall-runoff-turbidity dynamics of the study site (see Abbreviations of selected variables). Selected variables for correlation analysis were additionally checked for co-linearity using the Variance Inflation Factor. Cumulative particle size

distributions and the shape and oxidation level of sediment samples were used to examine spatial variability across the main stem and tributaries before and after the major event in August 2015. A Kruskal-Wallis test was applied to the sediment data to determine the statistical evidence of significant changes associated to the rainy and dry season events, and the major flood event (R core team, 2016).

3. Results

3.1 Rainfall-runoff event and turbidity dynamics

The study year was characterised by a record El Niño event (NOAA, 2016) resulting in lower than average annual precipitation (~2700 mm/yr, Table I). Despite the generally drier conditions on the Pacific slope, the catchment locally received a record convective rainfall event in August 2015 resulting in a likely > 50 yr return period flood event. A total of 29 rainfall events were selected over the study year from 13/06/2015 to 13/06/2016 (Figure 5, Table II). From the 26 hydro-meteorological variables, 8 (Table II, Abbreviations) were used to describe the temporal dynamics of events explaining 92 % of the total variance based on three Principal Components. The other 18 variables mostly resuming initial and recession conditions of events were neglected due to $r > 0.7$ indicating co-linearity. Furthermore, the 8 selected parameters showed small effects of co-linearity tested using the Variance Inflation factor resulting in values smaller than 6 for all cases. Table II gives the full spectrum of events and analysed variables with the overall mean and standard deviation.

As the hydrometerological conditions, in particular rainfall, are distinctly different for different seasons (Figure 1), we first describe the rainfall-runoff and turbidity event dynamics for each wet

297 and dry season cycle based on the typical climatic features of the study site. Out of the total 29
298 events, 25 occurred during the 2015 rainy season from June to December. During this rainy season,
299 the precipitation magnitude ranged from 2.8 to 132.3 mm, with average rainfall duration of 5.4
300 hours. The turbidity increased up to a maximum value in almost half of the events. The median
301 time lag between the rainfall peak and maximum discharge was one hour. The median time lag
302 between the discharge peak and the turbidity peak was also 1 hour, while the median time between
303 the peaks of precipitation and turbidity was 2.5 hours (Figure 5), but generally lags followed a
304 normal distribution.

305 During the dry season 2016 (January-April) only two out of the 29 events were identified (Figure
306 5), despite more sporadic rainfall originating from the Caribbean. The magnitude of the two
307 precipitation events was 19.3 and 45.2 mm (for the first and second event, respectively). The
308 discharge range reported was from 0.4 to 0.8 m^3/s and events lasted from 1.5 to 8.5 hours, while
309 the turbidity reached maximum values just once (Figure 5).

310 Likewise, also only two events were identified for the beginning of the rainy season in May 2016.
311 The magnitude *M* of these precipitation events was 12.7 mm and 35.6 mm (Table II). The discharge
312 range reported was 1.1 m^3/s and 1.7 m^3/s respectively, while the turbidity reached relatively low
313 values in both events (Figure 5).

314 The runoff-turbidity data showed distinctly different hysteresis patterns for periods before the main
315 August 2015 event and during the recovery period. The events before August 2015 did show few
316 hysteresis patterns exhibiting a clockwise behaviour (Table II; Figure 6, first panel). From August
317 2015, all events did indicate hysteresis patterns of discharge versus turbidity with changing
318 clockwise and anti-clockwise loops (Figure 6, second and third panel). The most frequent

hysteresis class according to the classification of Zuecco et al. (2016) was class 2 (clockwise, increasing from initial values, but shape of an eight similar to event 3, second panel of Figure 6). Apart from one class 6 and one class 5 event, no events that showed decreasing values from the initial state were detected (class 7 and 8). The hysteresis behaviour also shifted from no time lag to a relatively regular clockwise hysteresis including the major event in August (Figure 5, event 2) to a more chaotic anti-clockwise and eight-shaped hysteresis pattern, back to initial conditions showing a clockwise hysteresis (Figure 6, event 4).

3.2 Impacts of an extreme event on the rainfall-runoff response and turbidity dynamics

During August 2015, two consecutive convective storms in less than 36 hours triggered an estimated 50 yr return period flood event. Antecedent rainfall was 24 mm over 7 days with relatively dry soils before the first storm. On the first day, 132 mm of precipitation fell in less than 4 hours with a maximum intensity of 40 mm in 30 min (Figure 5, event 2). This storm caused water levels to rise 1.14 m with a discharge of around 25 m^3/s in less than 3.5 hours, with corresponding maximum turbidity levels of > 900 NTU.

The second event occurred 14 hours after the previous storm, with soil saturation at a maximum, and an additional accumulated 147 mm of rain in 4 hours. The maximum intensity was 77 mm in less than 30 min resulting in a water level increase of up to 2.86 m. The reconstructed flood peak discharge based on flood marks using Manning's equation resulted in approximately 370 ± 56 m^3/s. Turbidity levels were beyond 1000 NTU. A total accumulated rainfall of 279 mm revealed (post-event field inspections) important morphological changes in the river network and over 15 landslides contributing an estimated >100 m^3 of material were identified along the stream.

341 Tributaries were also intensively modified by incorporation of rocks, sediments, and vegetation
342 from the slopes (Figure 2E).

343

344 At the catchment level, the extreme flood event from August 2015 had some remarkable
345 consequences in terms of erosion and material transport (Figure 2A). The turbidity response to rain
346 events became slightly faster by around 30 min and reached maximum levels around 1000 NTU
347 with less precipitation after the flood event (Table II). The stream reached maximum turbidity
348 levels with on average lower precipitation inputs and rain intensity (Figure 5, event 3; Table II). A
349 Spearman rank correlation matrix was used to show differences in the time lag between the peaks
350 of precipitation, discharge and turbidity before and after the extreme event (Table III). The rainfall-
351 runoff dynamics before the extreme event were mostly related to antecedent conditions with a
352 significant correlation ($p<0.1$) of *AWI7* to discharge range (*Qrange*) of r = -0.66 and rainfall
353 intensity *Imax* to *Qrange* with r = 0.65. No significant correlations to lag times were detected prior
354 to the extreme event. The rainfall magnitude *M* and *Imax* were only moderately correlated to the
355 rainfall-runoff lag *P_Qlag* (r = -0.45) and the *P_NTUlag* with r=-0.42. The discharge range was
356 only moderately correlated to the turbidity range (*NTUrange*) (r = 0.58).

357

358 After the extreme flood event, the antecedent conditions played no role on rainfall-runoff and
359 turbidity dynamics (Figure 7b). However, the rainfall magnitude *M* was significantly correlated to
360 discharge ($r = 0.63$, $p < 0.05$), and correlated to *P_Qlag* (r = 0.36) and rainfall and discharge,
361 turbidity lag time (r = -0.4 and -0.48, respectively). The *P_Qlag* was also significantly related to
362 *Q_NTUlag* with r = -0.54 ($p < 0.1$) meaning the longer the rainfall-runoff response time is the

shorter the runoff-turbidity response. After the event, the *NTUrange* was significantly correlated to rainfall-turbidity lag time ($r = 0.56$, $p < 0.1$) and discharge-turbidity lag time (0.52, $p < 0.1$). A Kruskal-Wallis test was applied to the 8 selected variables before and after the event. The results of significance values p varied from 0.02 to 0.75 with the lag time of discharge to turbidity resulting in the only significant change at the 95 % level.

3.3 Sediment sources and connectivity

Soil erosion measurements:

Data recordings at the erosion pins showed that erosion was most prominently detected after the major event in August 2015 with a maximum soil loss and deposits of over 10 cm at various sites. However, the movement of materials in terms of erosion and deposition was variable across all sites. Figure 8 indicates that most material was mobilised towards the end of the rainy season (Figure 8 – M6, M7) with more accumulated rainfall. The erosion pins also showed that all sites were characterised by gaining and losing conditions at some point across variable 9 to 35 degrees steep slopes. Net erosion and net deposition was equally recorded at 5 sites each after the complete 1-year study period.

Figure 8 shows particle size distributions sampled from 1 week before and immediately 3 days after the extreme event for the main stem and three to four tributary streams on both hillslopes A and B (see Figure 3, sampling sites). The data for the main stem show that after the event, the dominant particle size was generally smaller (mainly medium to course sand), than prior to the

event (mainly coarse sand to gravel). Most tributaries (1A, 2A, 2B and 4B) showed a similar shift in behaviour after the event. In contrast, the tributaries 3A and 4A accumulated coarser grained material after the event, while the particle size distributions of tributaries 1B and 3B remained largely the same. The granulometric curves identified mainly coarse particle sizes and only less than 5% of all sediment samples collected were composed of silt. The latter material properties might also be related to a slightly different tributary catchment morphology with more moderate slopes (Figure 3) and finer material on hillslope A as opposed to coarser material on hillslope B.

Turbidity as an indicator of sediment loads:

Even though we focussed primarily on the temporal dynamics and potential processes that affect the rainfall-runoff-turbidity behaviour, we also explored the use of turbidity as an indicator for suspended sediment flux. Sediment particle size analyses from the 23 sampled storm events indicated that all sand and coarser material in the samples corresponded with turbidity measurements less than 200 NTU (Figure 9). Maximum turbidity exceeding 1000 NTU appeared to be generated by finer dissolved particles (fine sands and silt). In absence of a significant amount of superficially available clay particles (Figure 3c), the silt fraction was therefore responsible for most of the turbidity generated (Figure 9). The sand fraction did not result in turbidity higher than 50 NTU. However, silty material was less than 5 % of the stream sediment composition (pre- and post-event) and less than 30 % of hillslope soils in the catchment. Even small amounts of silt caused high turbidity independently of the total transported and sampled mass (Figure 9B). No relationship between turbidity, suspended sediment concentration SSC (g/L) and discharge was hence detected for construction of a reasonable rating curve during the study period (Figure 9A).

4. Discussion

4.1 Characterizing rainfall-runoff-turbidity dynamics in tropical, volcanic catchments

Among the first from humid tropical volcanic regions, our results showed that rainfall-runoff-turbidity dynamics in the San Lorencito catchment are driven by hydroclimatic conditions and can be further linked to heterogeneity in catchment characteristics and material properties of soils, and bedrock. The climatic seasonality exhibited a high inter-event variability of the rainfall-runoff-turbidity relationship particularly during the rainy season (Table II). The values of turbidity were generally higher during the months from May to December (Table II). The runoff generation in this steep and tropical setting causes - as can be expected (see Zimmermann et al., 2012) – a quick runoff response to rainfall inputs in the order of 30 to 40 min. However, there is an important surface runoff generation component (Dehaspe et al., 2018) contrary to other studies from similar systems that reported mostly sub-surface storm runoff generation (Muñoz-Villers and McDonnell, 2012). The rainfall-runoff response was unsurprisingly characterized by a significant relationship with the antecedent wetness and storm characteristics such as rainfall intensity, while we detected no significant rainfall-runoff-turbidity lags (Table III). However, the drivers of the rainfall-runoff response were less dominated by the wetness state of the catchment and rainfall intensity immediately after the impact of an extreme event that significantly modified the fluvial geomorphology of the catchment. In addition, there were significant lag times in the turbidity response to rainfall and discharge during that time. As such, we found complex discharge – turbidity hysteresis characteristics that shifted in shape and magnitude after the extreme event (Table III – Figure 6). It is likely that this can be explained by shifts in the sediment sources, which

428 in turn result in variations in the material itself (e.g. particle size, as shown by Cheraghi et al.
429 (2016)), but also the transport and delivery characteristics. Some events at the beginning of the
430 rainy season 2015 and before the extreme event did not show hysteresis, and others were
431 characterised by more complex temporal relationships (35 %). We observed mostly eight-shaped
432 hysteretic patterns (49 %) after the major flood event, while only 3 % of events showed positive
433 (clockwise) hysteresis in contrast to López-Tarazón and Estrany (2016) from a Mediterranean
434 catchment and 13 % showed negative (counter clockwise) hysteresis. Eight-shaped hysteresis
435 loops have previously been classified as less common and difficult to decipher in
436 geomorphologically different study areas (e.g. Hudson, 2003; Perks et al., 2015).

437

438 **4.2 The role of extreme events on sediment transport dynamics and fluvial geomorphology**

439 The transformation of fluvial systems mostly happens during extreme events, when equilibrium
440 river channel parameters and slope gradients may be disturbed and the thresholds controlling
441 fluvial or gravitational processes may be exceeded (Thomas, 1994). Among the hydro-
442 meteorological extreme events are those characterised by low exceedance probabilities of
443 precipitation and runoff. Even though our exceedance probability estimate of 50 years for the
444 August 2015 extreme event is rather uncertain, the empirical evidence suggested an extreme event
445 previously not observed for over 30 years. The orographic ascend of Caribbean trade winds
446 maintain a constant humidity most of the year with intense convective rainstorms originating from
447 the Pacific Ocean that caused the observed extreme runoff response and was the most intense
448 rainfall event of such a magnitude since measurements from 2008. The combination of both
449 precipitation mechanisms - a constant low intensity input of rainfall and intense convective storms

- causes saturation excess overland flow with possibly associated laminar erosion (in contrast to sub-surface stormflow generation on volcanic substrate identified by Muñoz-Villers and McDonnell, 2012 in Mexico). Material movement on the hillslopes was clearly detected by the erosion pins (Figure 8) particularly during the extreme event with soil losses and deposits of up to 10cm.

Furthermore, the San Lorencito stream is controlled by a system of parallel normal faults with SW-NE orientation; the direction in which the main channel drains (see Figure 1b, Denyer et al., 2003). Tectonic joints on the volcanic rocks can be observed along the stream channel outcrops, which is a pre-condition for exposed material and subsequent potential rapid incorporation into the stream in extreme conditions. The extreme event described above created alluvial deposits (in parts areas > 1800 m^2) along the riparian zone and removed riparian vegetation (Figure 2A). In addition, tributaries built up alluvial fans among deepening and widening of channels that caused the stream to abandon a certain stream section (Figure 2E). The flood debris flow deposited large amounts of material on abandoned fluvial terraces, and in other cases large deposits of young fluvial terraces where eroded (Figure 2F). The latter type of material close to the main channel can be incorporated and transported in short periods of time. Large rounded boulders such as in Figure 2F evidenced the torrential behaviour and stream capacity of recent and historic extreme events. Therefore, the study catchment can be characterised by an easy mobilisation of colluvial (mainly landslides and laminar soil erosion) and alluvial material (stream bank and terrace erosion). Nevertheless, such extreme events are part of the normal denudation on geological scales as suggested by deep scars of mass movement on the hillslopes (evidence from the elevation model in Figure 1) and large fluvial terraces (in parts with ~20 cm of pedogenesis in Figure 2F) strongly support recent Holocene torrential behaviour (Vargas, 1978).

473

474 **4.3 Sediment sources and hillslope-stream connectivity**

475 The periodic monitoring during sampling campaigns showed that the tributaries influence the
476 direction of streamflow and streambed incision (Figure 2E). The high rainfall in excess of 40 mm/h
477 in combination with variable geomorphological features of slope (e.g. on average lower slope on
478 hillslope A compared to B) and soils (Figure 3) and the vegetation density (Dehaspe et al., 2018)
479 dictated that the spatial variability of the catchment's connectivity was high (Fryers, 2013).

480 We also identified around 15 landslides that directly contributed colluvial material (> 100 m^3) into
481 the stream (Figure 2G and location in Figure 3). All rocks from the landslides were identified as
482 jointed andesites with different levels of profile weathering. After the stream lost transport capacity
483 during recession, the young incorporated material was deposited and readily available during
484 subsequent minor events causing high levels of turbidity for a prolonged time after peak flow (see,
485 e.g. Figure 5 - event 3). All the landslides identified during this study (Figure 3) occurred during
486 the rainy season. They also contributed an important amount of hillslope material into the stream
487 as part of or in addition to what was demonstrated by the monitored erosion pins (Figure 8).

488 Further evidence of hillslope-stream connectivity was found in identical levels of mineral
489 oxidation of sandy sediments recovered from soil, tributary and main stem sediment samples
490 (Figure S1). Seasonal patterns in sediment delivery, transport and deposition from the rainy season
491 into the dry season have been previously related to the rainfall regime with an increase in rainfall
492 events leading to an increased sediment yield (Thomas, 1994; Fryers, 2013). This is in agreement
493 with our results, even though we were limited by only using soil erosion measurements and
494 turbidity as an indicator for temporal dynamics in suspended sediments. Nevertheless, the transit

of material from the hillslopes to the stream and within the channel appeared to occur throughout the year, even though the frequency of rainfall events was less during the dry season. Such high rainfall probability despite a climatic seasonality occurred similarly in other catchments on the south Pacific slope (Birkel et al., 2016). During the dry season, drying soils allowed for relatively more water to infiltrate (Figure 5b – dry season rainfall events did result in very minor runoff response), limiting the means for particles to erode from the hillslopes (Figure 8). The relatively slow and limited sediment movement during the dry season was therefore dominated by readily available material stored in the channel or from channel erosion since the channel sediments were mostly sands with less than 5% fine sandy aggregates (Figure 7) and these particles have a higher settling velocity than the silts and clays originating from the hillslopes. Much of the hillslope sediment movement with erosion and deposition was generated during the rainy season (Figure 8).

Sediment monitoring revealed two main types of sediment sources to the stream: Firstly, hillslope material that was fed into the stream and tributaries through landslides, colluvial, and surface erosion (similar to agricultural sites in the tropics, Duvert et al., 2010). Secondly, material deposits that formed fluvial terraces and sediment banks in areas of low stream power. The sediment particle distributions of the main stem and tributaries revealed that these were mostly coarse sand and gravel particles (~95 %). The fine sand and coarse silt particles represented less than 5 % of all sediment samples (see Figure 9). Sediments also exhibited an intense oxidation and weathering of minerals (composed primarily by Phenocrystals such as plagioclase, augite, magnetite, hornblende, quartz, olivine, biotite) similar to the dominating sand-silt soil samples as shown in Figure 3 and S1. Similarities found in terms of morphology, particle size distribution, mineralogy and oxidation of sands provided evidence of a hillslope – stream connection mainly due to erosion caused by periodic surface runoff generation under more extreme rainfall (Figure 5). The most

likely mechanism was saturation excess overland flow (Dehaspe et al., 2018), since soils throughout the catchment have high infiltration capacities in excess of 200 mm/h (in contrast to Zimmermann et al., 2012). Under such extreme conditions, the dense forest cover does not play a significant role on flood generating runoff mechanisms anymore (e.g. Birkel et al., 2012 from another tropical volcanic Costa Rican catchment) that can also be associated to dominate material transport in steep, tropical, volcanic catchments.

Contrary to other extra-tropical studies (e.g. Hudson, 2003; Rovira and Batalla, 2006), we excluded a sediment exhaustion effect over the year. In the San Lorencito catchment, sediments seemed to always be available and constantly moving, even though there was sediment depletion over the dry season due to less rainfall events, increased infiltration of soils and the interception effect of the vegetation cover on the hillslopes. It might well be that sediment availability is key for rapid landscape transformations in the humid, volcanic tropics. However, more measurements combining sediment fingerprinting similar to Duvert et al. (2010) and Martínez-Mena et al. (1999) with efforts to quantify loads and their particle size distribution over a longer period will be necessary to confirm these initial results.

5. Conclusions and outlook

The challenge of working in tropical environments is partly reflected in less monitored catchments on a global scale. For example, the recent global review on erosion and sediment dynamics in the tropics by Labriere et al. (2015) did not include any study from Central America as an indication of the under-represented monitoring in the region. Apart from the study by Jansson (2002) that looked at event-scale SSC – Q hysteresis to determine sediment sources and the large-scale study

by Krishnaswamy et al. (2001), there are to the best of our knowledge no systematic high-temporal resolution studies reported in the literature. Ziegler et al. (2014) estimated the uncertainty in SSC – Turbidity data from Thailand to be a major source of error in high load estimates over longer periods. In that sense, sensor equipment with a large NTU range (0 to 10000 NTU) is needed to capture the complete variability of runoff – turbidity events. Such events need to be accompanied by high-resolution sediment sampling with an appropriate sampling strategy that captures the complete particle size classes from fine to coarse material.

The hillslope – stream connectivity can only quantitatively be assessed with automatic measurements of eroded material volumes and particles from the hillslopes at the same (or close) temporal sampling resolution. Our soil erosion measurements adapted from Hancock and Lowry (2015) in combination with a morphometric analysis of soils and sediments provided some evidence of such a hillslope – stream connectivity. However, estimates of erosion rates will need either a process-based model analysis using our preliminary data or a sediment fingerprinting in form of e.g. radioisotope analysis and/or a combination of both to further explore and quantify sediment loads and land-forming processes.

This study aimed to gain more insights into the spatio-temporal variability of sediment sources, availability, and transport dynamics in humid tropical volcanic landscapes via intense monitoring. The study emphasized the importance of combined hydro-geomorphic data collection using high temporal resolution sensors and basic synoptic surveys of soil erosion and sediment material properties. In summary, our results indicated that sediment transport dynamics in steep humid tropical volcanic areas, as represented by the study catchment, are highly dynamic by nature

against a background of high but unquantified sediment loads. Generally, sediments were supplied to the stream from the hillslopes in the form of laminar erosion triggered by saturation excess overland flow. However, extreme events with the occurrence of landslides exert an overriding impact on sediment dynamics even with 100% primary rainforest cover. In response to such an extreme event, runoff-turbidity relationships switched from a non-hysteretic to a strongly hysteretic behaviour after the extreme event. Nevertheless, our results indicated that the system of sediment dynamics was very resilient, as the post-event recovery was relatively quick (around 3 months). We also found that during our preliminary monitoring in the tropical, tertiary volcanic environment of the study site, turbidity and discharge are only weak indicators of sediment load and no meaningful discharge – SSC rating curve could be developed (Figure 9). This might limit the use of turbidity data for use of sediment load studies in these environments, but we need more data over much longer measurement periods to be affirmative.

We conclude that more studies are needed in tropical, volcanic catchments to provide high-resolution baseline data for process-based model development applied to inform water users such as e.g. hydropower companies about the natural sediment load dynamics and budgets of headwater catchments that provide much of the ecosystem services used downstream. This study provided important first insights into the timing of sediment dynamics and allowed for the formulation of preliminary hypotheses of sediment sources and transport mechanisms. However, to quantify these aspects of hillslope-stream connectivity, we need to combine high temporal resolution monitoring over longer time periods with high spatial resolution erosion and sediment measurements. Remotely sensed imagery from LiDAR-equipped drone applications and radioisotopes for sediment fingerprinting might help in this regard and allow us to quantitatively assess

584 geomorphological changes to stream networks and their transport rates in tropical, volcanic
585 catchments.

586

587 **Acknowledgements**

588 A British Geomorphological Society early career grant to JG and CB allowed initiating this work.
589 An Ideawild grant to CB contributed with an equipment donation. The University of Costa Rica
590 Research Council (projects B4239, B8709) supported this project. We thank the ReBAMB staff
591 and students for helping with logistics and fieldwork. The data can be obtained upon request from
592 the corresponding author.

References

American Public Health Association, American Water Works Association, Water Environment Federation. 1999. Standard methods for the examination of water and wastewater. United States.

Bergoeing, J.P., 2007. Geomorphology of Costa Rica. Librería Francesa: San José, Costa Rica.

Birkel, C., Soulsby, C., Tetzlaff, D., 2012. Modelling the impacts of land cover change on streamflow dynamics of a tropical rainforest headwater catchment. Hydrological Sciences Journal. DOI: 10.1080/02626667.2012.728707.

Birkel, C., Geris, J., Molina, M.J., Mendez, C., Arce, R., Dick, J., Tetzlaff, D., Soulsby, C., 2016. Hydroclimatic controls on non-stationary stream water ages in humid tropical catchments. Journal of Hydrology. 542, 231-240. DOI: 10.1016/j.jhydrol.2016.09.006.

Bonell, M., Bruijnzeel, L.A., 2005. Forests, Water and People in the Humid Tropics. Cambridge University Press: Cambridge. DOI: 10.1017/CBO9780511535666.020.

Bracken, L.J.,Wainwright, J., Ali, G.A., Tetzlaff, D., Smith, M.W., Reaney, S.M., Roy, A.G., 2013. Concepts of hydrological connectivity: Research approaches, pathways and future agendas. Earth-Science Reviews. 119, 17-34. DOI: 10.1016/j.earscirev.2013.02.001.

Buendia, C., Vericat, V., Batalla, R.J., Gibbins, C.N., 2015. Temporal dynamics of sediment transport and transient in-channel storage in a highly erodible catchment. Land Degradation & Development. 27, 1045–1063. DOI: 10.1002/ldr.2348.

Calvo, J., 1998. Suspended sediment yield prediction models for Costa Rican watersheds. International Association of Hydrological Sciences. 253, 27–32.

Chang, J.H., Lau, L.S., 1983. Definition of the humid tropics. In Hydrology and Water Management in the Humid Tropics, Bonell M, Hufschmidt MM, Gladwell JS (eds.). Cambridge University Press: Cambridge; 571–575.

Chappell, N.A., Douglas, I., Hanapi, J.M., Tych, W., 2004. Sources of suspended sediment within a tropical catchment recovering from selective logging. Hydrological Processes. 18, 685–701. DOI: 10.1002/hyp.1263.

Cheraghi, M., Jomaa, S., Sander, G.C., Barry, D.A., 2016. Hysteretic sediment fluxes in rainfall-driven soil erosion: Particle size effects. Water Resources Research. 52, 8613-8629. DOI: 10.1002/2016WR019314.

Chow, V.T., 1959. Open channel hydraulics. McGraw-Hill, New York.

Dehaspe, J., Birkel, C., Tetzlaff, D., Sánchez-Murillo, R., Durán-Quesada, A.M., Soulsby, C., 2018. Spatially distributed tracer-aided modelling to explore water and isotope transport, storage

and mixing in a pristine, humid tropical catchment. Hydrological Processes. 32, 3206– 3224. https://doi.org/10.1002/hyp.13258.

Denyer, P., Montero, W., Alvarado, G.E., 2003. Atlas tectónico de Costa Rica. UCR: San José.

Downing, J.A., Cole, J.J., Duarte, C.M., Middelburg, J.J., Melack, J.M., Prairie, Y.T., Kortelainen, P., Striegl, R.G., McDowell, W.H., Tranvik, L.J., 2012. Global abundance and size distribution of streams and rivers. Inland Waters. 2, 229–236. DOI: 10.5268/IW-2.4.502.

Duvert, C., Gratiot, N., Evrard, O., Navratil, O., Némery, J., Prat, C., Esteves, M., 2010. Drivers of erosion and suspended sediment transport in three headwater catchments of the Mexican Central Highlands. Geomorphology. 123, 243-256. DOI: 10.1016/j.geomorph.2010.07.016.

Fagan, M.E., DeFries, R.S., Sesnie, S.E., Arroyo, J.P., Walker, W., Soto, C., Chazdon, R.L., Sanchun, A., 2013. Land cover dynamics following a deforestation ban in northern Costa Rica. Environmental Research Letters. 8. DOI: 10.1088/1748-9326/8/3/034017.

Foley, J.A., DeFries, R., Asner, G.P., Barford, C., Bonan, G., Carpenter, S.R., Chapin, F.S., Coe, M.T., Daily, G.C., Gibbs, H.K., Helkowsky, J.H., Holloway, T., Howard, E.A., Kucharik, C.J., Monfreda, C., Patz, J.A., Prentice, C., Ramankutty, N., Snyder, P.K., 2005. Global Consequences of Land Use. Science. 309. DOI: 10.1126/science.1111772.

Fryers, K., 2013. (Dis)Connectivity in catchment sediment cascades: a fresh look at the sediment delivery problem. Earth Surface Processes and Landforms. 38, 30-46. DOI: 10.1002/esp.3242.

Giorgi, F. 2006. Climate change hot-spots. Geophysical Research Letters. 33. DOI: 10.1029/2006GL025734.

González, J.E., Georgescu, M., Lemos, M.C., Hosannah, N., Niyogi, D., 2017. Climate change's pulse is in Central America and the Caribbean. Eos 98. DOI: 10.1029/2017EO071975.
Hancock, G.R., Lowry, J.B.C., 2015. Hillslope erosion measurement --a simple approach to a complex process. Hydrological Processes. 29, 4809–4816. DOI: 10.1002/hyp.10608.

Henríquez, C., Cabalceta, G., 2012. Guía práctica para el estudio introductorio de los suelos con un enfoque agrícola. Costa Rican Association of Soil Science: San José.

Hudson, P.F., 2003. Event sequence and sediment exhaustion in the lower Panuco Basin, Mexico. Catena. 52, 57-76. DOI: 10.1016/S0341-8162(02)00145-5.

Jansson, M., 2002. Determining sediment source areas in a tropical river basin, Costa Rica. Catena. 47, 63-84.

Krishnaswamy, J., Halpin, P.N., Richter, D.D., 2001a. Dynamics of sediment discharge in relation to land-use and hydro-climatology in a humid tropical watershed in Costa Rica. Journal of Hydrology. 253, 91-109. DOI: 10.1016/S0022-1694(01)00474-7.

672 Krishnaswamy, J., Richter, D., Halpin, P., Hofmockel, M., 2001b. Spatial patterns of suspended
673 sediment yields in a humid tropical watershed in Costa Rica. Hydrological Processes. 5, 2237-
674 2257. DOI: 10.1002/hyp.230.
675
676 Labrière, N., Locatelli, B., Laumonier, Y., Freycon, V., Bernoux, M., 2015. Soil erosion in the
677 humid tropics: A systematic quantitative review. Agriculture, Ecosystems & Environment. 203,
678 127-139. DOI: 10.1016/j.agee.2015.01.027.
679
680 Loescher, H.W., Powers, J.S., Oberbauer, S.F., 2002. Spatial variation of throughfall volume in an
681 old-growth tropical wet forest, Costa Rica. Journal of Tropical Ecology. 18, 397-407. DOI:
682 10.1017/S0266467402002274.
683
684 López-Tarazón, J.A., Estrany, J., 2017. Exploring suspended sediment delivery dynamics of two
685 Mediterranean nested catchments. Hydrological Processes. 31, 698– 715.
686 DOI: 10.1002/hyp.11069.
687
688 Martínez-Mena, M., Alvarez-Rogel, J., Albaladejo, J., Castillo, V., 1999. Influence of vegetal
689 cover on sediment particle size distribution in natural rainfall conditions, in a semiarid
690 environment. Catena. 38, 175–190.
691
692 Mills, C.F., Bathurst, J.C., 2015. Spatial variability of suspended sediment yield in a gravel-bed
693 river across four orders of magnitude of catchment area. Catena. 133, 14-24.
694 https://doi.org/10.1016/j.catena.2015.04.008.
695
696 Muñoz-Villers, L.E., McDonnell, J.J., 2012. Runoff generation in a steep, tropical montane cloud
697 forest catchment on permeable volcanic substrate. Water Resources Research. 48. DOI:
698 10.1029/2011WR011316.
699
700 NOAA., 2016.
701 http://www.cpc.ncep.noaa.gov/products/analysis_monitoring/ensostuff/ensoyears.shtml (last
702 visited July 2017).
703

704 Norambuena, P., Luzio, W., Vera, W., 2002. Comparison between the pipette and bouyoucos
705 methods and their relation with water retention in eight soils of the andean plateau, Parinacota
706 Province, Chile. Agricultura Técnica. 62. DOI: 10.4067/S0365-28072002000100015.

707 Perks, M.T., Owen, G.J., Benskin, C.M., Jonczyk, J., Deasy, C., Burke, S., Reaney, S.M.,
708 Haygarth, P.M., 2015. Dominant mechanisms for the delivery of fine sediment and phosphorus
709 to fluvial networks draining grassland dominated headwater catchments. Science of the Total
710 Environment. 523, 178-190. DOI: 10.1016/j.scitotenv.2015.03.008.

711 R Development Core Team. 2016. R: A Language and Environment for Statistical Computing. R
712 Foundation for Statistical Computing: Vienna.
713

714 Rovira, A., Batalla, R.J., 2006. Temporal distribution of suspended sediment transport in a
715 Mediterranean basin: The Lower Tordera (NE Spain). Geomorphology. 79, 58-71. DOI:
716 10.1016/j.geomorph.2005.09.016.

717 Salazar-Rodríguez, A.H., 2003. Reserva Biológica Alberto Manuel Brenes: Una excepción en
718 Costa Rica. Revista InterSedes 8.
719
720 Shanley, J.B., McDowell, W.H., Stallard, R.F., 2011. Long-term patterns and short-term
721 dynamics of stream solutes and suspended sediment in a rapidly weathering tropical watershed.
722 Water Resources Research. 47. DOI: 10.1029/2010WR009788.
723
724 Sharon, D., 1980. The distribution of hydrologically effective rainfall incident on sloping
725 ground. Journal of Hydrology. 46, 165-188. DOI: 10.1016/0022-1694(80)90041-4.
726
727 Thomas, MF., 1994. Geomorphology in the Tropics: A Study of Weathering and Denudation in
728 Low Latitudes. John Wiley and Sons: Chichester.
729

730 Tricart, J., 1965. Principes et méthodes de la géomorphologie. Masson et Cie Éditeurs: Paris.

731 Vargas, G., 1978. Diagnóstico y recomendaciones para el manejo y ordenamiento de los recursos
732 naturales de la cuenca del río San Lorenzo, Alajuela, Costa Rica (unpublished thesis). University
733 of Costa Rica.
734

735 Veas, N., 2009. Caracterización y estimación de la erosión laminar en un bosque pre-montano a
736 partir de un modelado hidrológico. Microcuenca del río San Lorencito, Cordillera Volcánica de
737 Tilarán, Costa Rica. (unpublished thesis). University of Costa Rica.

738 Walsh, R.P.D., Bidin, K., Blake, W.H., Chappell, N.A., Clarke, M.A., Douglas, I., Ghazali, R.,
739 Sayer, A.M., Suhaimi, J., Tych, W., Annammala, K.V., 2011. Long-term responses of rainforest
740 erosional systems at different spatial scales to selective logging and climatic change.
741 Philosophical Transactions of the Royal Society London B Biological Sciences. 366 (1582),
742 3340–3353. DOI: 10.1098/rstb.2011.0054.

743 Wohl, E., Barros, A., Brunsell, N., Chappell, N., Coe, M., Giambelluca, T., Goldsmith, S.,
744 Harmon, R., Hendrickx, J., Juvik, J., McDonnell, J., Ogden, F., 2012. The hydrology of the
745 humid tropics. Nature Climate Change. 2, 655-662. DOI: 10.1038/nclimate1556.

746 Zhang, Z., Tao, F., Shi, P., Xu, W., Sun, Y., Fukushima, T., Onda, Y., 2010. Characterizing the
747 flush of stream chemical runoff from forested watersheds. Hydrological Processes. 24(20), 2960
748 - 2970. DOI: 10.1002/hyp.7717.

749 Ziegler, S.G. Benner, C. Tantasirin, S.H. Wood, R.A. Sutherland, R.C. Sidle, N.R.A. Jachowski,
750 X. Lu, A. Snidvongs, T.W. Giambelluca, J.M. Fox. 2014. Turbidity-based sediment monitoring
751 in northern Thailand: hysteresis, variability, and uncertainty. Journal of Hydrology. DOI:
752 10.1016/j.jhydrol.2014.09.010.

Zimmermann, A., Francke, T., Elsenbeer, H., 2012. Forests and erosion: Insights from a study of suspended-sediment dynamics in an overland flow-prone rainforest catchment. Journal of Hydrology. 27, 170-181. DOI: 10.1016/j.jhydrol.2012.01.039.

Zuecco, G., Penna, D., Borga, M., van Meerveld, H.J., 2016. A versatile index to characterize hysteresis between hydrological variables at the runoff event timescale. Hydrological Processes. 30, 1449-1466. DOI: 10.1002/hyp.10681.

TABLES

Table I. Basic catchment descriptors and data properties for hydro-meteorological and geomorphologic context.

Descriptor	Unit	Mean [Range]
Area	km^2	3.2
Topography		
Elevation	m.a.s.l.	1133.5 [873.7-1472.4]
Slope	°	22.3 [0.15-52]
Drainage Density (1:200000)	km/km^2	0.016
Stream Slope	°	20.5
Sediment Transport Index		17.04 [0-390]
Terrain Ruggedness Index		1.63 [0.01-5.03]
Hydroclimatic		
Annual P 2015-2016	mm	2762
Annual PET 2015-2016	mm	425
Annual Q 2015-2016	mm	2448

Table II. The hydro-meteorological characteristics (8 variables) of the selected rainfall events during the study period (co-linear variables were removed) plus the hysteresis index of Zuecco et al. (2016) and classification are shown. The four events marked in italics were used for further analysis and note that the second (extreme) event marks the pre- and post-event periods used in the analysis. The mean and standard deviation was calculated without the August 2015 extreme event. The selected variables were a 7-day Antecedent Wetness Index – *AWI7d*, rainfall magnitude *M*, maximum rainfall intensity – *Imax*, discharge event range – *Q range*, lag time from rainfall peak to discharge peak – *P_Qlag*, turbidity event range – *Range*, lag time from rainfall peak to turbidity peak – *P_TUlag*, lag time from turbidity peak to discharge peak – *TU_Qlag*.

Event Date	AWI7d (mm)	M (mm)	Imax (mm/h)	Q range (m^3/s)	P_Qlag (h)	Range (NTU)	P_TUlag (h)	TU_Qlag (h)	Hyst index	Hyst Class
13-14/6/2015	74.89	13.21	13.21	0.34	1	587.66	6	6	0.063	2
16-18/6/2015	68.55	29.71	8.64	1.16	1	998.08	2.5	1.5	*	*
1) 19-20/6/2015	59.4	8.38	3.58	0.69	1.5	69.09	2.5	1	*	*
24-25/6/2015	58.87	22.05	7.36	0.79	7	413.01	8.5	1.5	*	*
26/6/-2/7/2015	75.84	26.63	3.55	1.26	13.5	463.3	13.5	0	0.036	2
7-8/7/2015	42.81	38.08	19.3	3.08	3.5	204.4	0.5	0.5	0.065	2
10-11/7/2015	91.26	28.95	18.54	0.75	1	84.24	3.5	2.5	*	*
14-15/7/2015	127.32	2.78	2.03	1.69	2	786.55	2.5	0.5	-0.576	4
19-21/7/2015	39.5	25.13	22.1	4.2	1	580.82	4	3	-0.098	4
29-30/7/2015	29.11	56.65	27.43	17.25	0.5	704.43	-3.5	-2	0.545	1
8-10/8/2015	24.53	132.33	40.13	4.99	2.5	813.05	2.5	0	0.341	1
2) 10-11/8/2015	158.64	98.57	77.22	343.77	0	974.06	1	1	0.126	1
31/8-1/9/2015	8.61	59.19	29.72	1.75	0.5	929.61	1.5	1	-0.124	3
11-12/9/2015	55.34	44.95	32.51	9.62	1	760.64	7.5	6.5	0.11	1
13-14/9/2015	106.89	38.1	29.47	3.89	1.5	636.58	0.5	-1	0.186	2
17-18/09/2015	93.93	10.16	9.66	1.4	1	762	2	1	-0.32	4
19-20/09/2015	56.82	4.32	4.07	1.34	0.5	854.2	3	2.5	-0.558	4
20-21/09/2015	22.03	10.92	6.61	0.8	1	425	2.5	1.5	0.039	2
21-22/09/2015	32.2	48.01	32.52	14.3	1	722.1	1	0	0.127	1
22-23/09/2015	80.96	35.05	25.4	3.73	0.5	939.1	4	3.5	0.205	2
3) 27-28/09/2015	126.67	34.79	33.02	6.68	0.5	877.4	7	6.5	0.036	1
12-13/10/2015	76.82	8.64	5.59	1.11	1	906.9	9.5	8.5	0.213	5
16-18/10/2015	76.61	49.77	26.67	10.7	1.5	327.5	0	-1.5	0.215	1
20-23/10/2015	90.59	50.3	21.59	7.03	7.5	636.8	1.5	-6	0.033	2
05-07/11/2015	28.39	35.56	19.56	4.33	0.5	508.2	0.5	0	0.086	2
31/12/2015 - 02/01/2016	8.59	19.29	4.83	0.76	2.5	997.2	4.5	2	-0.628	4
27/4/2016	6.59	45.22	40.39	0.47	1	57.9	6	5	0.32	6
4) 26-27/5/2016	9.33	12.69	11.68	1.12	1.5	222.42	1.5	0	0.064	2
31/5-2/6/2016	34.73	35.56	31.5	2.72	1	191.77	0.5	-1	-0.016	3
Mean:	*57.4*	*33.1*	*18.9*	*3.9*	*2.1*	*587.9*	*3.4*	*1.5*		

Std. Dev.:	*35.0*	*25.4*	*12.1*	*4.4*	*2.8*	*298.6*	*3.5*	*3.0*		

*no hysteretic behaviour detected.

Table III. Pre-event (upper panel in Grey italics) and post-event (lower panel in black) Spearman rank correlation matrix of eight selected rainfall-runoff-turbidity parameters. Statistical significance is given by asterisks (* = 90%, ** = 95% and *** = 99%).

	AWI7d (mm)	M (mm)	Imax (mm/h)	Qrange (m^3/s)	P_Qlag (h)	Range (NTU)	P_TUlag (h)	TU_Qlag (h)
AWI7d (mm)	1	*-0.61 (*)*	*-0.84 (**)*	*-0.66 (*)*	*0.13*	*-0.19*	*0.34*	*0.27*
M (mm)	**-0.01**	1	*0.81 (**)*	*0.58 (*)*	*-0.19*	*0.33*	*-0.46*	*-0.42*
Imax (mm/h)	**0.1**	**0.71 (**)**	1	*0.65 (*)*	*-0.41*	*0.22*	*-0.4*	*-0.1*
Qrange (m^3/s)	**0.47**	**0.63 (**)**	**0.48**	1	*-0.17*	*0.58 (*)*	*-0.42*	*-0.52*
P_Qlag (h)	**-0.13**	**0.36**	**-0.1**	**-0.03**	1	*-0.19*	*0.44*	*-0.24*
Range (NTU)	**0.4**	**-0.42**	**-0.38**	**0.01**	**-0.23**	1	*-0.19*	*-0.27*
P_TUlag (h)	**-0.01**	**-0.4**	**-0.07**	**-0.4**	**-0.28**	**0.56 (*)**	1	*0.45*
TU_Qlag (h)	**-0.04**	**-0.48**	**-0.03**	**-0.38**	**-0.54 (*)**	**0.52 (*)**	**0.93 (***)**	1

FIGURES

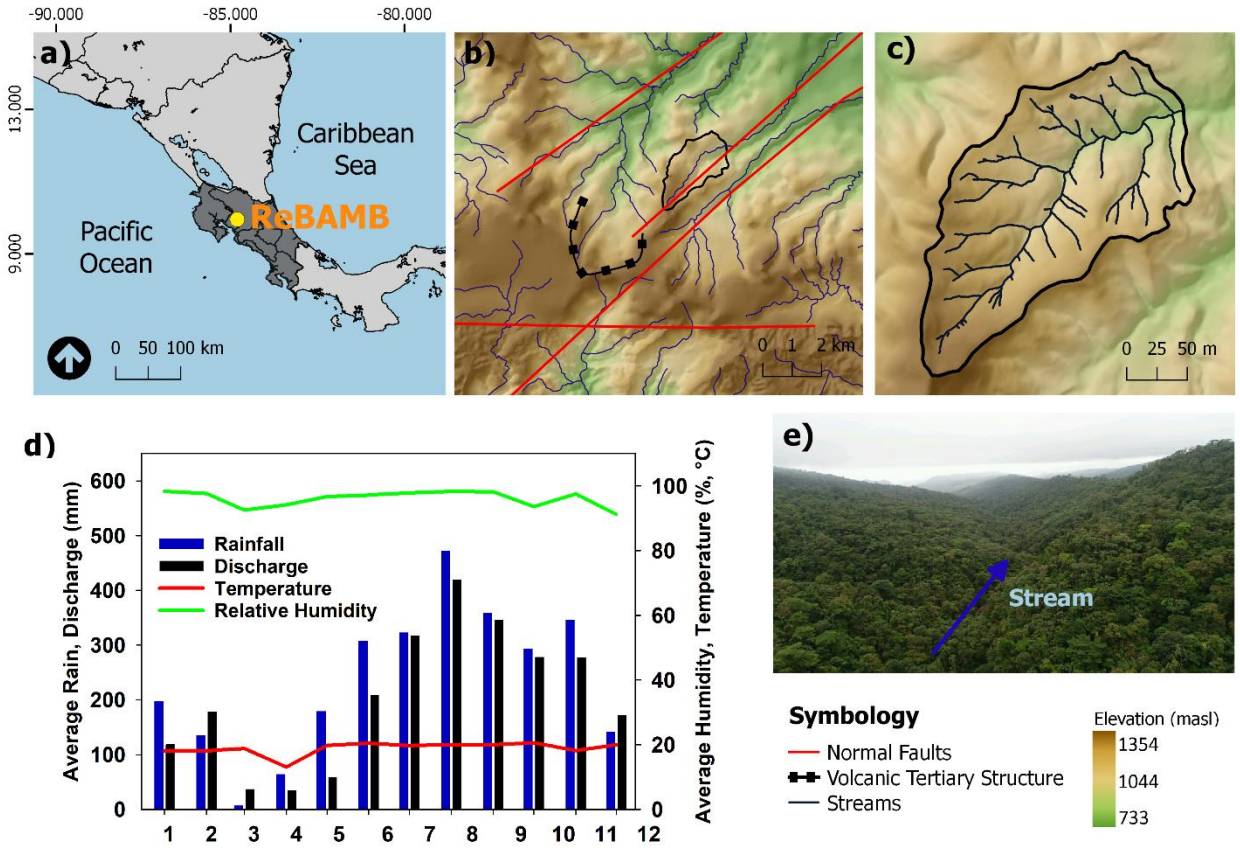

Figure 1. a) Regional context showing the location of the San Lorencito catchment in Costa Rica, Central America with b-c) topography, volcanic, and tectonic geological features (fault lines and the tertiary volcano remnant) that affect sediment dynamics (Denyer et al., 2003), d) monthly climate regime from January to December (1 to 12) based on the measurements of 2015-2016, and e) aerial image of the dense rainforest.

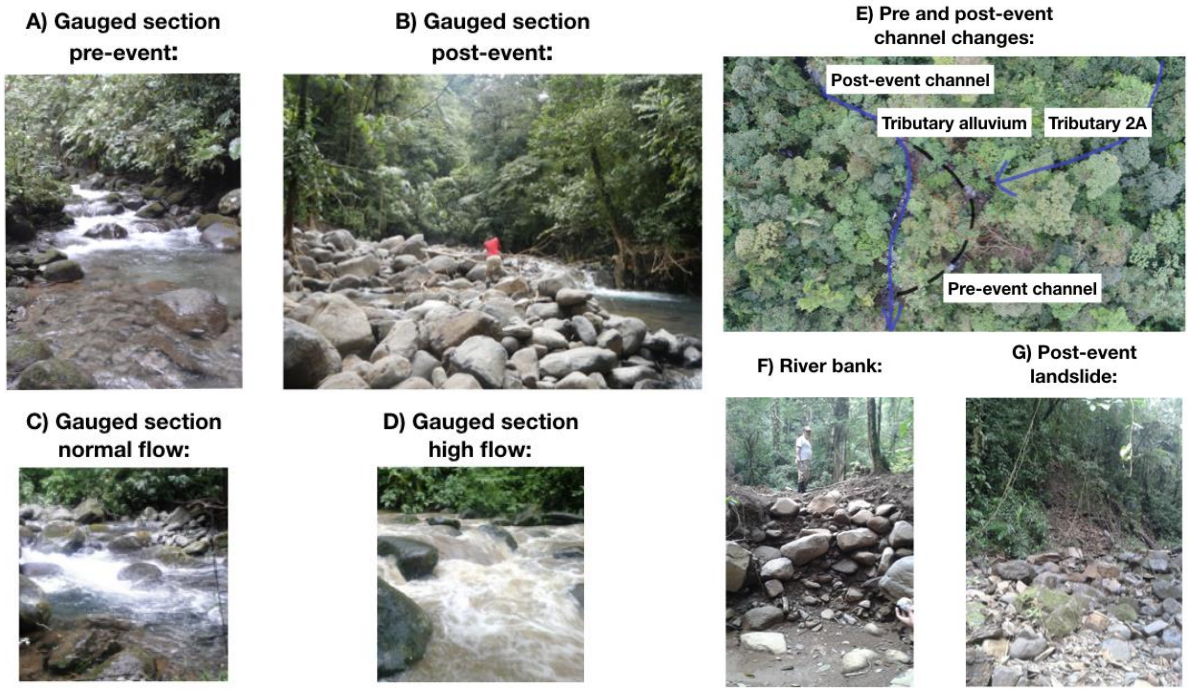

Figure 2. A and B) The pre-event step-pool stream morphology looking upstream from the gauged section and the widened post-event section with material deposits. C and D) show the flow in normal conditions and high flow with turbid water. E) Reconstructed stream channel modifications and the tributary influence in contributing alluvial material. F) Post-event eroded stream bank showing the previously deposited fluvial material. G) Post-event landslide incorporating fresh material into the stream.

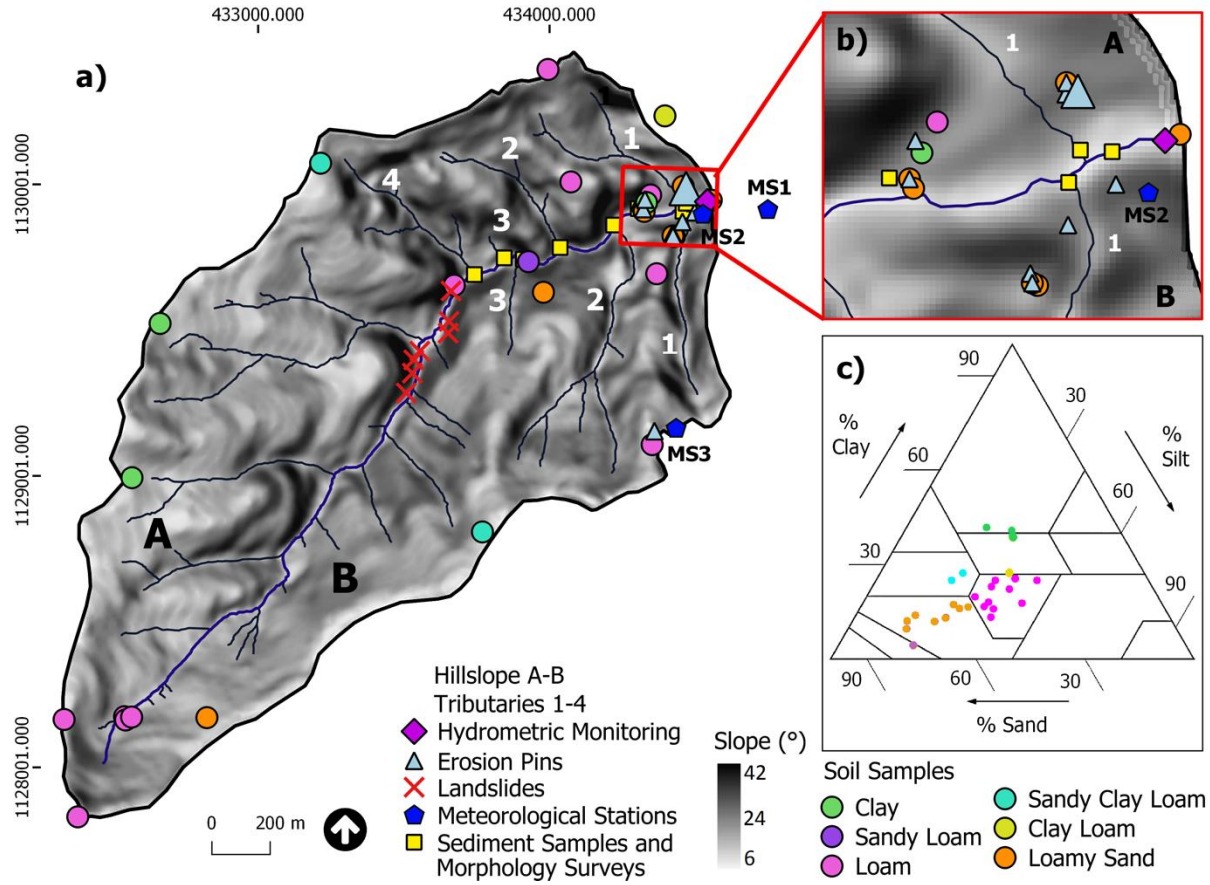

855

856 **Figure 3.** a) The slope map (grey scale) shows the location of monitoring equipment
857 (hydrometric and meteorological stations MS with MS1 recording gross precipitation and MS2
858 and MS3 throughfall) and spatial surveys, b) the detailed map indicates the locations of soil,
859 erosion (larger triangle shows the largest soil erosion measurement), landslides and sediment
860 surveys dictated by site access, and c) the distribution of the processed and colour coded soil
861 samples across the United States Department of Agriculture (USDA) texture triangle.

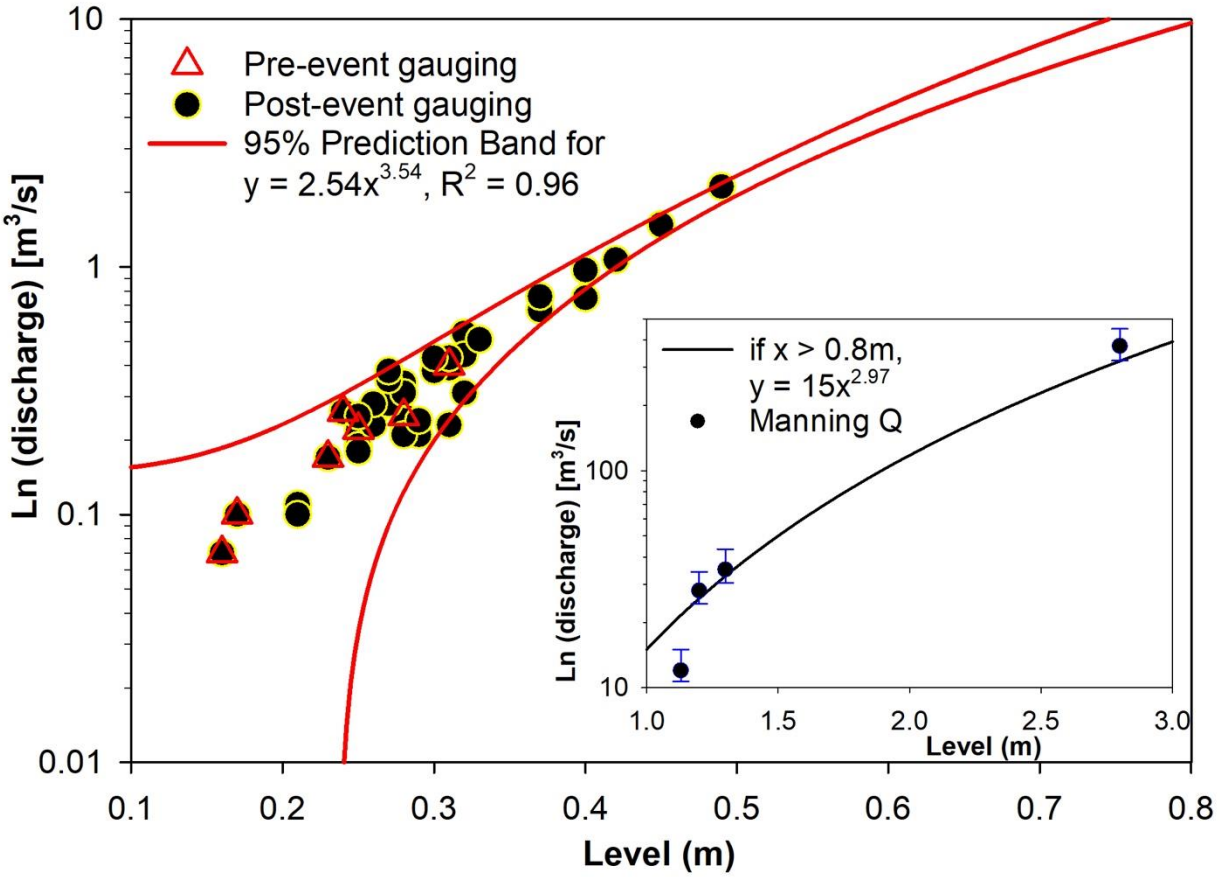

862

863 **Figure 4**. The preliminary two-stage rating curve for the San Lorencito stream based on 37

864 manual gaugings (7 pre-event in red triangles and 30 post-event in yellow-black circles) and four

865 re-constructed largest peak flows with overbank flow using Manning's equation (inlet graph).

866 The error bars were calculated systematically varying Manning's n roughness coefficient.

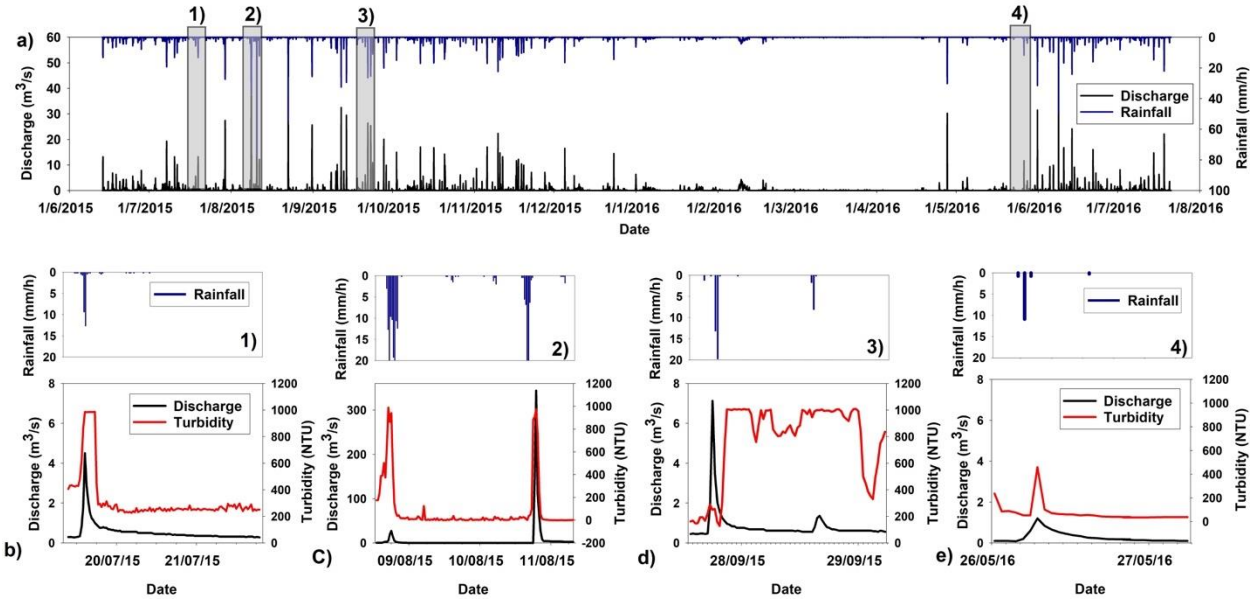

867

868 **Figure 5.** a-b) Average hourly rainfall-runoff time series for the study period with four selected
869 events marked with grey bars emphasizing the discharge-turbidity dynamics during 1) the rainy
870 season before the extreme event, 2) the major event in August 2015, 3) post-event during the rainy
871 season and 4) at the beginning of the rainy season in May 2016. All scales are comparable apart
872 from the major event (2) occurred in August 2015 showing a different scale for visualization
873 purposes.

874

875

876

877

878

879

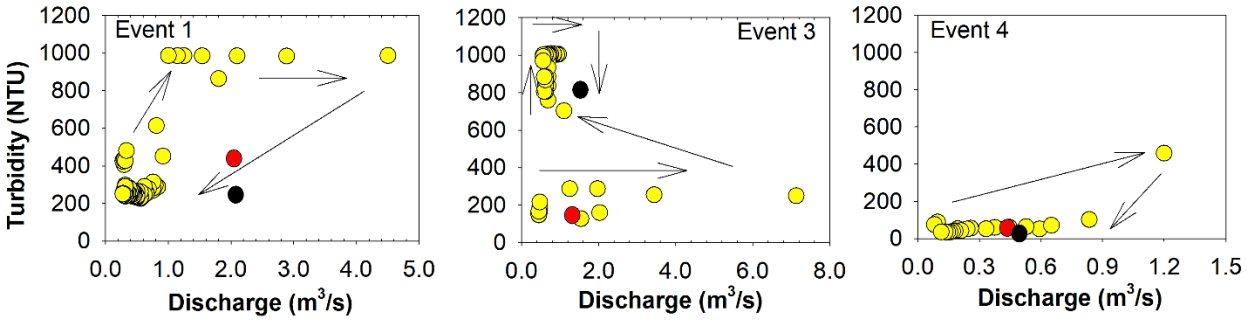

880

881 **Figure 6.** Discharge – turbidity hysteresis plots for pre-flood event (event 1 in Figure 4) conditions
882 (clockwise hysteresis), post-flood event (event 3 – anti-clockwise and eight-shaped hysteresis) and
883 recovery conditions (event 4 – clockwise hysteresis). The turbidity scale is comparable for
884 visualization purposes and the numbering of events corresponds to Figure 4. Red dots mark the
885 starting discharge and turbidity, black dots indicate the end of the event and the arrows give the
886 hysteresis direction.

887

888

889

890

891

892

893

894

895

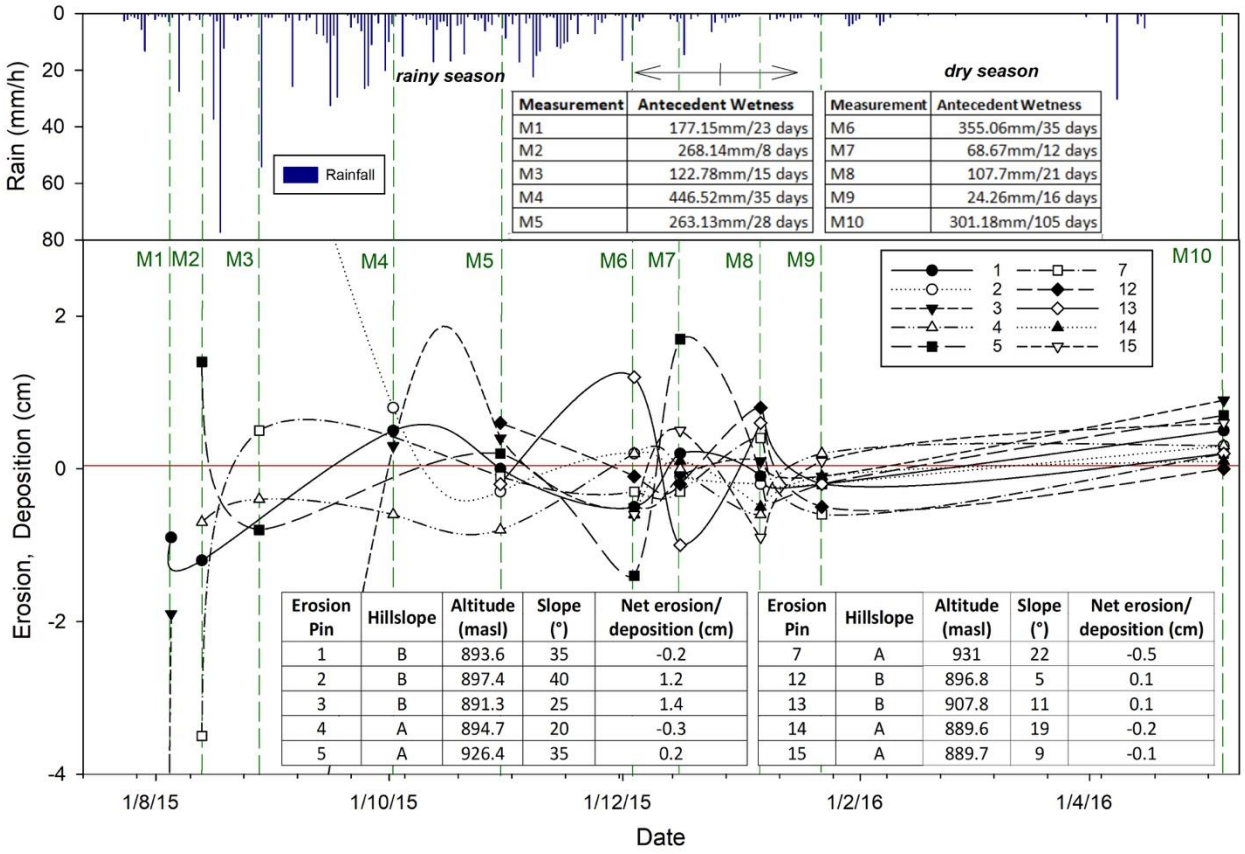

Measurement	Antecedent Wetness
M1	177.15mm/23 days
M2	268.14mm/8 days
M3	122.78mm/15 days
M4	446.52mm/35 days
M5	263.13mm/28 days

Measurement	Antecedent Wetness
M6	355.06mm/35 days
M7	68.67mm/12 days
M8	107.7mm/21 days
M9	24.26mm/16 days
M10	301.18mm/105 days

Erosion Pin	Hillslope	Altitude (masl)	Slope (°)	Net erosion/ deposition (cm)
1	B	893.6	35	-0.2
2	B	897.4	40	1.2
3	B	891.3	25	1.4
4	A	894.7	20	-0.3
5	A	926.4	35	0.2

Erosion Pin	Hillslope	Altitude (masl)	Slope (°)	Net erosion/ deposition (cm)
7	A	931	22	-0.5
12	B	896.8	5	0.1
13	B	907.8	11	0.1
14	A	889.6	19	-0.2
15	A	889.7	9	-0.1

Figure 7. Soil movement was detected using erosion pins for the study period 2015-16 with the sites (see Figure 2) main physical characteristics (slope and altitude) and the accumulated rainfall between measurements. Negative values represent erosion and positive values represent deposition (accumulation of material). The measurements were connected with smoothed lines to emphasize the temporal variability over the roughly monthly interval. Erosion pin 3 showed the largest soil erosion and pin 2 the largest deposition (both on hillslope B).

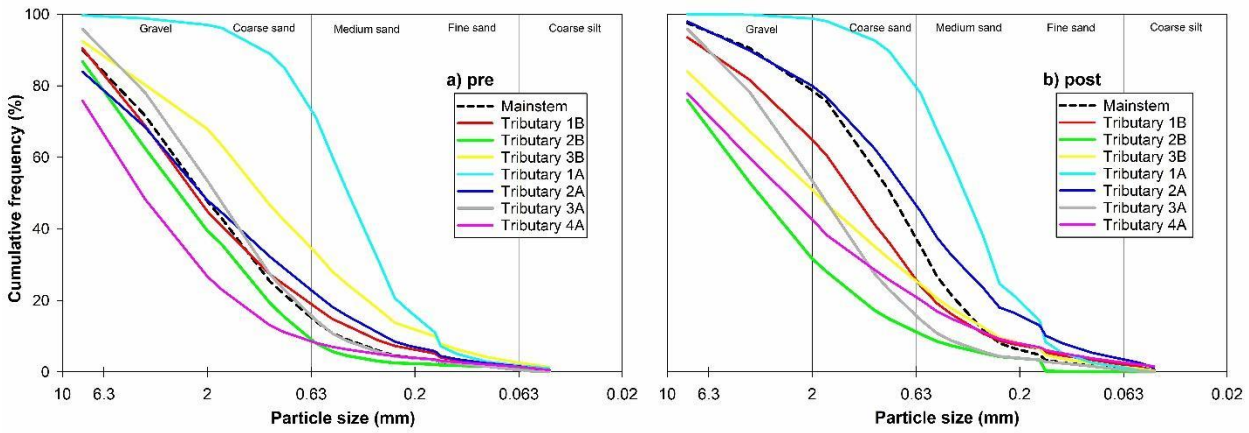

903

904 **Figure 8.** The figure shows the particle size distributions of stream sediments sampled a) before
905 and b) after the major flood event across the drainage network and tributaries as indicated in
906 Figure 2 (A, B corresponds to the hillslope location and the increasing numbering of upstream
907 tributaries).

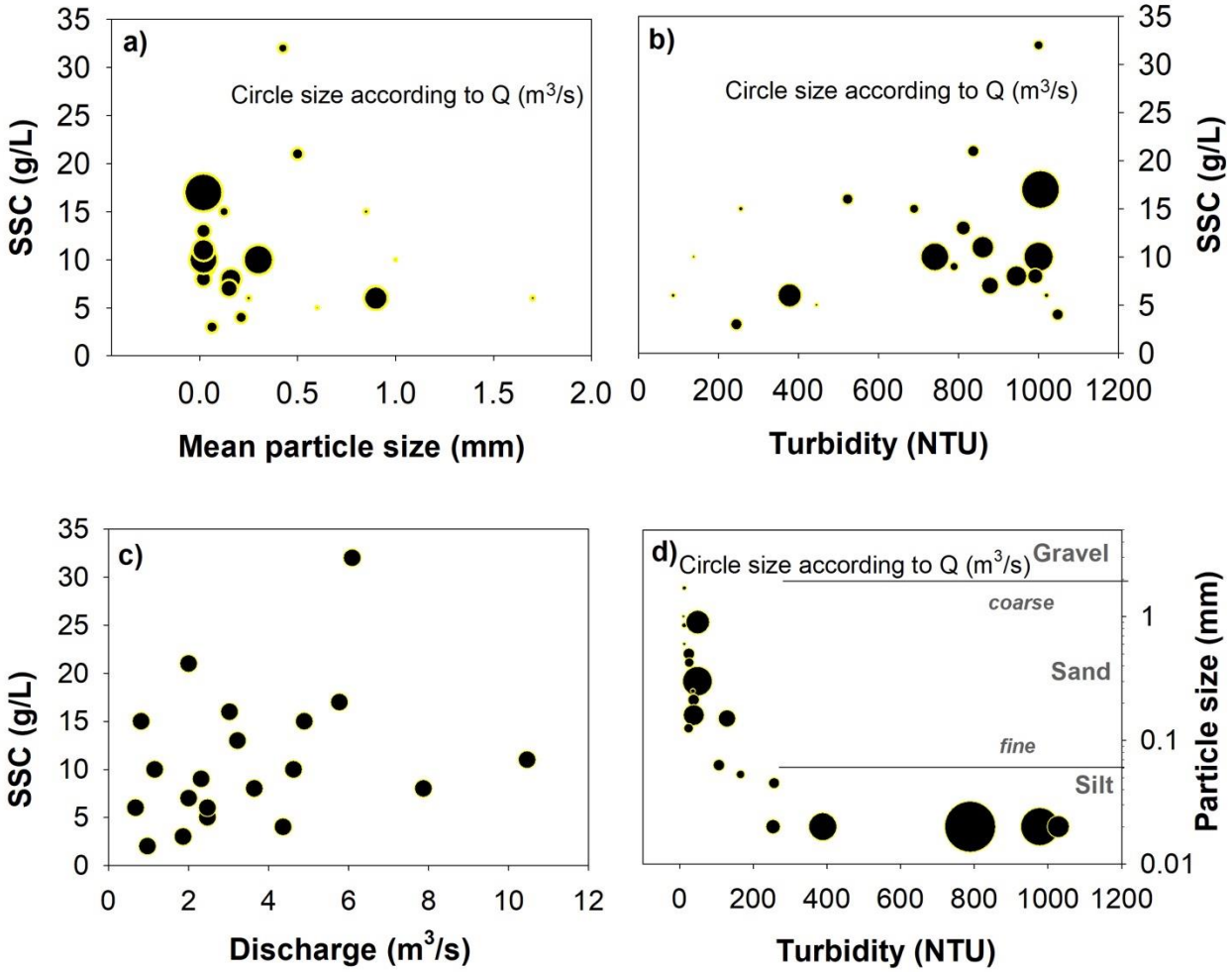

908

909 **Figure 9.** a) the mean particle size – suspended sediment concentration (SSC in g/L) – discharge
910 (Q) visualization from 0.2 to 10 m^3/s is plotted for 23 storm event samples and b) the SSC and
911 turbidity level.

912

913

914

915

SUPPLEMENTARY MATERIAL

Figure S1. Direct stereo microscope comparison of fine sands material properties (angle, oxidation level) recovered from an exemplary soil sample (left hand side) and stream sediment sample of tributary 1B (right hand side). Note that the soil sample was taken from within the contributing sub-catchment area of tributary 1B and shows almost identical mineralogy in support of a hillslope-stream connectivity.